International Journal of High-Rise Buildings
September 2021, Vol 10, No 3, 229-242
https://doi.org/10.21022/IJHRB.2021.10.3.229

International Journal of
High-Rise Buildings
www.ctbuh-korea.org/ijhrb/index.php

Dynamic Characteristics and Responses of Tall Building Structures with Double Negative Stiffness Damped Outriggers

Feifei Sun[1,2], Ningling Duan[2], Meng Wang[2], and Jiaqi Yang[2†]

[1]State Key Laboratory of Disaster Reduction in Civil Engineering, Tongji University, China
2 Department of Structural Engineering, Tongji University, China

Abstract

Dynamic characteristics of tall building structures with double negative stiffness damped outriggers (2NSDO) are parametrically studied using the theoretical formula. Compared to one negative stiffness damped outrigger (1NSDO), 2NSDO can achieve a similar maximal modal damping ratio with a smaller negative stiffness ratio. Besides, the 2NSDO can improve the maximum achievable damping ratio to about 30% with less consumption of an outrigger damping coefficient compared to the double conventional damped outriggers (2CDO). Besides, the responses of structures with 2NSDO under fluctuating wind load are investigated by time-history analysis. Numerical results show that the 2NSDO is effective in reducing structural acceleration under fluctuating wind load, being more efficient than 1NSDO.

Keywords: Negative stiffness, Double damped outrigger, Modal damping ratio, Vibration control

1. Introduction

The negative stiffness device (NSD) can provide a force whose direction is the same as the relative motion between its two terminals, so this device is able to assist the relative motion between its two terminals. During the last decade, many negative stiffness devices (Pasala et al. 2013, 2014, 2015; Sarlis et al. 2013; Shi and Zhu 2015; Sun et al. 2017) or pseudo-negative stiffness devices (Iemura and Pradono 2009; Wang et al. 2018) were passively realized and tested. Many studies directly adopted the linear negative stiffness to improve the performance of isolated buildings (Kwon et al. 2016), stayed cables (Chen et al. 2015), multistory buildings (Qu et al. 2017), and tuned mass dampers (Antoniadis et al.2016; Nagarajaiah 2009; Sapountzakis et al. 2017).

Based on the characteristic of the NSD, Wang et al. (Wang et al. 2019) proposed a negative stiffness amplifying damper (NSAD) by paralleling the NSD with the dashpot of the Maxwell damping element (MED). The NSAD utilized the NSD to amplify the relative motion of the dashpot, which led to the amplification of the damping ability of the dashpot. Wang et al. proposed the closed-form expressions of optimal parameters for an undamped SDOF system with an NSAD by fixed point method. And he found that the NSAD with optimal parameters improved the energy dissipation capacity by 5-16 times, causing 40~60% of seismic response reduction for most structural period range. Besides, Wang et al. (Wang et al. 2019) introduced the NSAD into the MDOF system and found that the NSAD could reduce the maximal peak inter-story drift by about 30%.

For the application of NSD in tall buildings, a negative stiffness damped outrigger (NSDO) was proposed by paralleling an NSD with the damper of conventional damped outrigger (CDO) to further improving the damping effect of the existing tall buildings with flexible perimeter columns. (Wang et al. 2021) In the NSDO, the NSD, the viscous damper, and the perimeter column made up an NSAD together, achieving damping amplification. Wang et al. found that NSDO significantly improved the modal damping ratio for each structural mode with much less consumption of the outrigger damping coefficient than the CDO. And under fluctuating wind load, the NSDO could further decrease the maximum acceleration response of CDO structures by over 50% with the same consumption of viscous dampers at the outrigger. In the meantime, the NSDO achieved a similar or better performance as the CDO did in mitigating interstory drift responses. Sun et al. (Sun et al. 2021) also found that the structure retrofitted by NSDO decreased the harmful drift and structural acceleration of over 51% and 29% respectively for real earthquakes and saves the damping cost by 85.9% simultaneously compared with the structure with CDO. Therefore, the NSDO has a significant application value in structural retrofitting of actual engineering structures with CDO.

To the best of the authors' knowledge, the existing investigation of NSDO only concentrates on the fundamental characteristics of the one-NSDO (1NSDO) model and the performance of one-CDO (1CDO) structures retrofitted by the NSD. However, for the actual engineering structures, more than one CDO is needed to control the vibration

†Corresponding author: Jiaqi Yang
E-mail: yjqjarvis@tongji.edu.cn.

responses to satisfy the vibration mitigation requirement of structures. Therefore, to retrofit the double-CDO (2CDO) structures of actual engineering, it is necessary to investigate the dynamic characteristics and the performance of double negative stiffness damped outriggers (2NSDO) structures. In this paper, a double outriggers model is used to study the dynamic characteristics of 2NSDO structures. Modal damping ratios and modal frequencies are parametrically studied to show the influences of outrigger damping, negative stiffness ratios, stiffness ratios of a core tube-to-column, and outrigger positions. In addition, the vibration mitigation effect of structures using 2NSDO is studied under wind loads.

2. The Basic Mchanism of Negative Stiffness Amplifying Damper

2.1. The simplified model of brace-viscous damper system

The viscous damper (VD) is a conventional energy dissipation component that provides the additional damping ratio for structures and dissipates the input energy. In the actual engineering, the supporting brace is usually used to connect the VD with the upper story and lower story, which uses the interstory drift of structure to push the VD, as shown in Fig. 1. In most cases, the stiffness of the supporting brace can not be ignored, so the whole brace-viscous damper system should be analyzed when an engineer designs a VD. In this way, if the supporting brace is equivalent to an axial spring with elastic stiffness k_p, and the VD is assumed as a dashpot, the brace-viscous damper system can be described as the most simplified theoretical model - the Maxwell damping element (MDE) whose axial spring is in series with the dashpot, as shown in Fig. 1.

The schematic diagram of MDE is shown in Fig. 2, when the viscous coefficient $C_d=\infty$, joints i and s are locked, which means there is no relative motion between joint i and s. In this condition, the MDE can be regarded as an elastic spring without any energy dissipation. In contrast, when $C_d=0$, the damping force is zero, the MDE can not dissipate energy either. From the two extreme

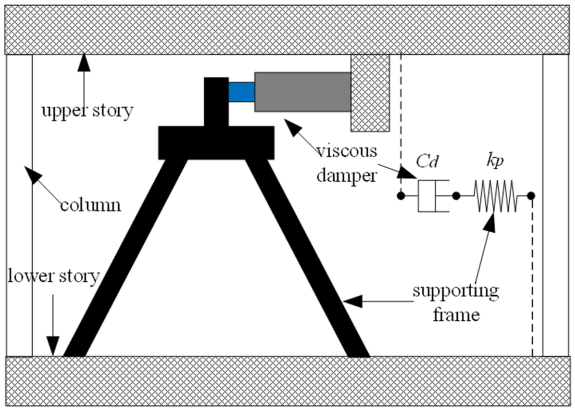


Figure 1. Conventional configuration of a VD.

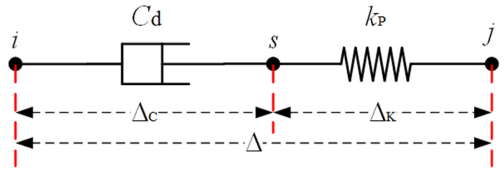


Figure 2. Schematic diagram of MDE.

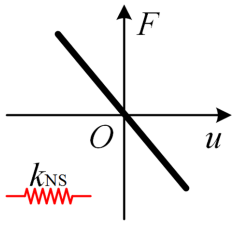


Figure 3. Negative stiffness spring.

conditions mentioned above, there will be an optimal C_d causing maximal dissipated energy. However, it also means that the energy dissipation capacity of MDE corresponding to the optimal C_d can not be further improved only by increasing or decreasing the damping coefficient.

2.2. The concept of negative stiffness mechanism

The negative stiffness device (NSD) can be equivalent to a negative stiffness spring with negative stiffness k_{NS} in this paper, as shown in Fig. 3. Different from the positive stiffness spring, the slope of the force-displacement curve of the negative stiffness spring is negative, which means the direction of negative stiffness force is the same as that of the relative motion of the two terminals in the negative stiffness spring. Therefore, the negative stiffness spring assists the relative motion of its two terminals. In other words, the more relative movement of NSD develops the more negative stiffness force increases, which in turn promotes the relative motion of NSD. And this characteristic is called the deformation assisting effect.

2.3. The concept of the negative stiffness amplifying damper (NSAD)

Based on the deformation assisting effect of NSD, the NSD can be introduced into the MDE by paralleling connected with the dashpot of the MDE to further improve the damping ability of MDE, as shown in Fig. 4(a). Because the NSD is paralleled connected with the dashpot, the relative motions of these two elements are the same, and the deformation assisting effect of the NSD can be used to amplify the relative motion of the dashpot. Therefore, the dissipated energy of NSAD is larger than that of the MED, as shown in Fig. 4(b).

3. The Dynaimc Characteristices of Structures with 2NSDO

3.1. The simplified model of structure with 2NSDO

A double-pair outrigger model based on the Euler-

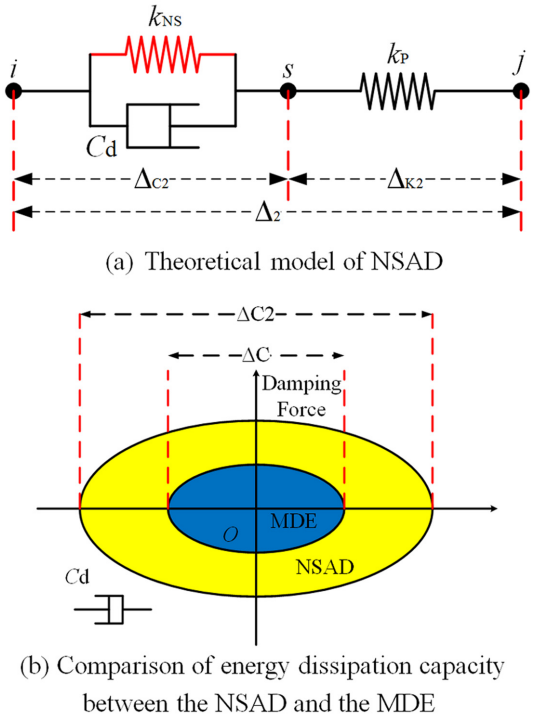


Figure 4. Schematic diagram of NSAD.

Bernoulli beam model is used to study the dynamic characteristics of structures with 2NSDO. As shown in Fig. 5, the core tube is equivalent to an Euler-Bernoulli beam with a bending stiffness *EI*, distributed mass *m*, length *r*, and height *H*. Two symmetrical outriggers with an infinity bending stiffness are implemented between the core tube and column of the perimeter frames. The perimeter columns are divided into *3* parts by *2* outriggers. The axial stiffness of each part of the column is represented by the spring $k_{ci}(i=1,2)$. And the axial stiffness is calculated as $k_{c1}=\frac{E_cA_c}{\alpha_1 H}$ and $K_{c2}=\frac{E_cA_c}{(\alpha_2-\alpha_1)H}$, where E_c is Young's modulus; A_c is the section area of the perimeter columns; and α_i is the normalized position ratio for each outrigger $(i=1,2)$. Besides, $C_{di}(i=1,2)$ is the damping coefficient of VD in each part of the perimeter column.

As shown in Fig. 5, the VDs are applied between outrigger ends and perimeter columns to provide energy dissipation. And an extra NSD with negative stiffness $k_{NSi}(i=1,2)$ is paralleled connected to the VD to further improve the damping effect of VD. The NSD, the VD, and the perimeter column make up an NSAD. The stroke of the VD $(u_i-u_{ci}(i=1,2)$ would be amplified, because the negative stiffness assists the deformation of its two terminals rather than resists it.

3.2. Modal damping ratios and frequencies

According to Wang et al.'s study (Wang et al. 2021), the 1NSDO can achieve a relatively large modal damping ratio of the first mode when the outrigger is located at the

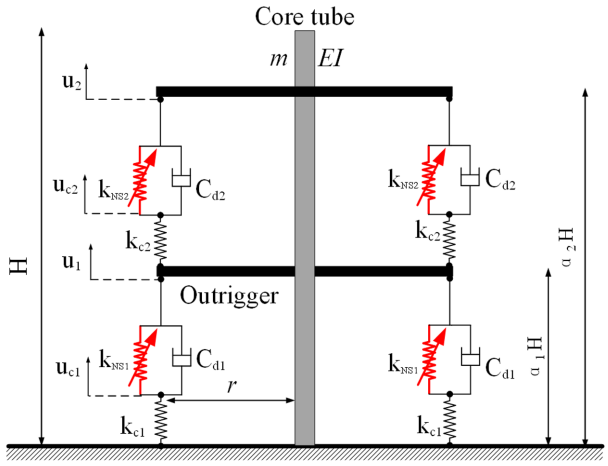


Figure 5. Simplified model for 2NSDO.

top of the core tube. Therefore, the authors use the structures with 2NSDO (the first NSDO is located at the middle of the core tube, the second NSDO is located at the top of the core tube), that is the simplest structure in structures with 2NSDO, to investigate the influence of an extra NSDO on damping ability of the 1 NSDO structure. Based on this simple 2NSDO structure, the structure equipped with 2NSDO shown in Fig. 5 can be simplified as a cantilever column with an intermediate rotational spring, as shown in Fig. 6.

According to the Duan's work (Duan 2021), the Eigen equation of the equivalent analytical model based on the Euler-Bernoulli beam theory can be given:

$$\frac{1}{\lambda}(k_{O11}D_{11}+2k_{O12}D_{12}+k_{O22}D_{22}) + \frac{1}{\lambda^2}(k_{O11}kO_{22}-k_{O12}O_{12})D_d+D_k=0 \quad (1)$$

where, $k_{Oij}(i=1,2;j=1,2)$ is the element of a 2×2 rotation stiffness matrices of 2 NSDO with two rotation freedom, which is the function of viscous coefficients of NSDO $c_i=\frac{C_{di}r^2}{H\sqrt{mEI}}(i=1,2)$, the stiffness ratio of core tube-to-

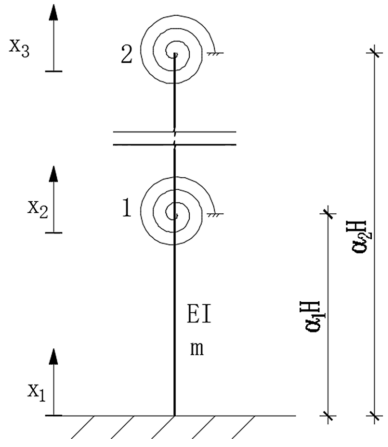


Figure 6. Equivalent analytical model for 2NSDO system.

column $\beta=\frac{EI}{2E_cA_cr^2}$ and the negative stiffness ratios of the NSD $\eta_i=\frac{k_{NSi}}{k_{ci}}i=(1,2)$. And $D_{ij}(i=1,2;j=1,2)$, D_k, and D_d are the functions of the normalized position ratio for the first outrigger α and the eigenvalue λ.

The Eq.(1 can be solved by the Newton-Raphson method (Wang et al. 2021) to calculate the eigenvalue of each mode λ_p. And then, the modal frequency can be calculated as:

$$\omega_p=\lambda_p^2\sqrt{\frac{EI}{ML^4}}(p=1,2\cdots) \tag{2}$$

The complex frequencies (Tan et al. 2015) can be obtained:

$$i\omega_p=i\lambda_p^2\sqrt{\frac{EI}{ML^4}}=-\xi_p\omega_{np}+i\sqrt{1-\zeta_p^2}\omega_{np}(p=1,2\cdots) \tag{3}$$

where ω_{np} is pseudo-undamped natural circular frequency, and $i=\sqrt{-1}$. And the modal damping ratio ζ_p is:

$$\xi_p=\frac{Re(i\omega_p)}{\omega_{np}}(p=1,2\cdots) \tag{4}$$

3.3. Parametric study

In this part, the modal damping ratios and frequencies of the NSDO structures are parametrically studied using Eq.(1 to evaluate the influence of NSDO parameters. The dynamic characteristics of 2NSDO system are compared with that of the 2CDO, 1NSDO, and 1CDO systems. Detailed parameters of the NSDO are listed in Table 1. For the case of $\eta_1=0$ and $\eta_2=0$, the studied 2NSDO degraded to 2CDO. For the case of $\eta_2=0$, and $c_1=0$, the 2NSDO degraded to 1NSDO. For the case of $\eta_1=0$, $\eta_2=0$, and $c_2=0$, the 2NSDO degraded to 1CDO.

3.3.1 The Influence of Outrigger Damping

The influence of outrigger damping on the modal damping ratios and frequencies ratio of 2NSDO, 2CDO, 1NSDO, and 1CDO structures are presented in Fig. 7. With the increase of the outrigger damping c, the modal damping ratios provided by the 2NSDO, 2CDO, 1NSDO, and 1CDO increase firstly and decrease later; the modal frequencies gradually increase and then remain constant. This is because the increase of the outrigger damping coefficient benefits the modal damping ratio at a low degree. However, if the outrigger damping is too significant, the stroke of the VD will be decreased seriously and locked. In this case, the CDO gradually equals to a CO, which provides an extra stiffness but little additional damping.

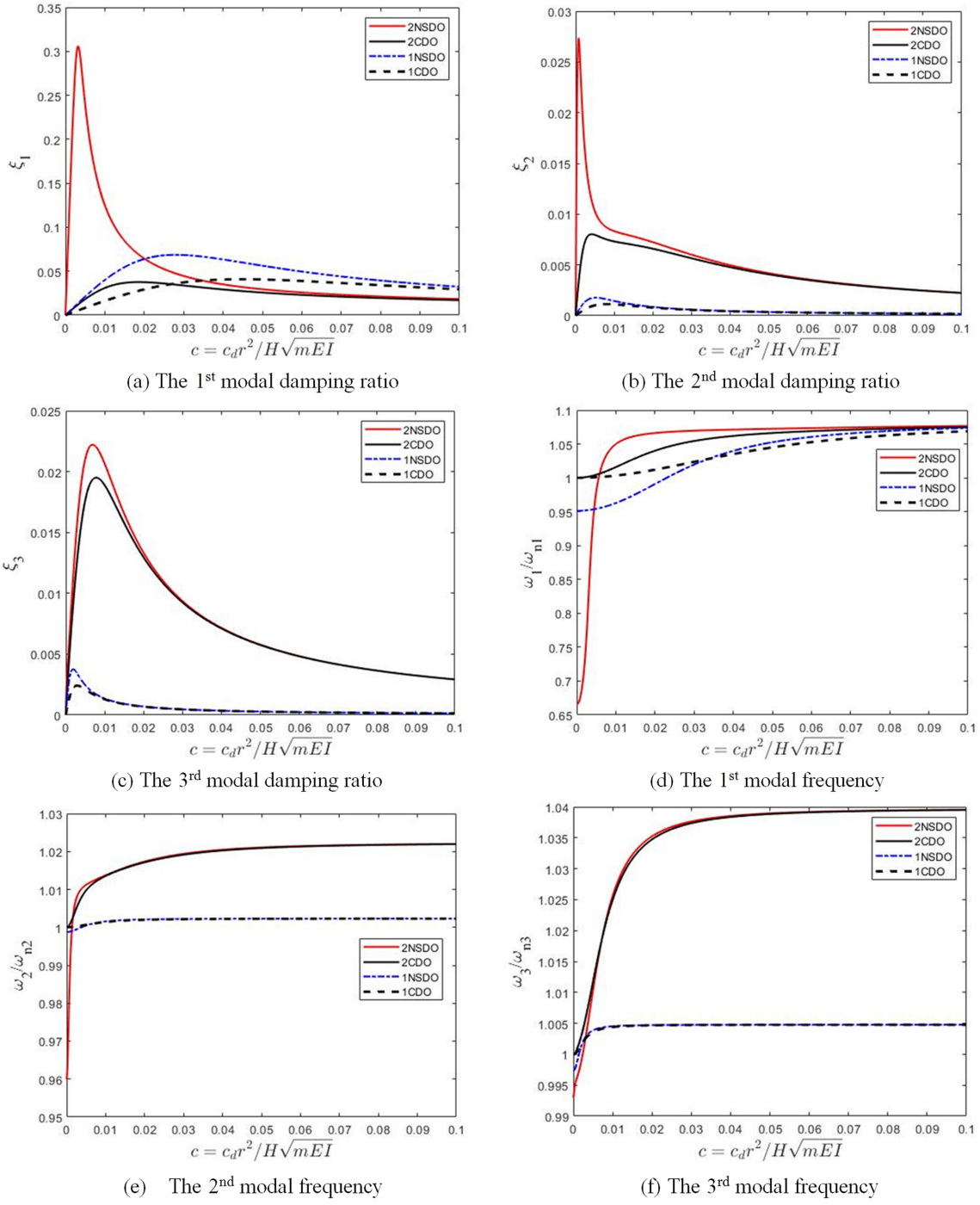
As shown in Fig. 7(a)-Fig. 7(c), because the stiffness ratio of the core tube-to-column is $\beta=5.0>3.7$, the modal damping ratio provided by the 2CDO and 1CDO for the first mode is always lower than 5%, no matter how much of the outrigger damping coefficient is selected, which is consistent with the work of Tan (Tan et al. 2015). We should notice that the maximum achievable damping ratio can be significantly improved by introducing the NSD. For instance, the 2NSDO could achieve a prominent damping ratio (over 30%) for the first mode, despite the insufficient stiffness of the perimeter column. The maximum achievable damping ratio of 2NSDO (over 30%) is much larger than 1NSDO (6.8%) for the first mode. And the c of 2NSDO corresponding to the maximum achievable damping ratio is 0.0034, while that of the 1NSDO is 0.008. Therefore, 2NSDO can use a less outrigger damping to achieve a more significant modal damping ratio compared with 1NSDO. In addition, according to Wang's study, (Wang et al. 2021) if the modal damping ratio of the first mode achieves 30% in 1NSDO, the negative stiffness ratio η_1 should be –0.75, which is hard to achieve in practical engineering. Fortunately, the 2NSDO only needs 46.6% of the negative stiffness of the 1NSDO to realize the same first modal damping ratio of 30%, which largely simplifies the application of NSDO. Overall, compared with the 1NSDO, the use of the 2NSDO achieves a larger damping ratio with a much smaller demand for both the negative stiffness and outrigger damping.

In addition, to achieve a large damping ratio, the stiffness ratio of the core tube-to-column β in 2CDO and CDO should be lower than 0.5 (Tan et al. 2015), which means the axial stiffness of perimeter columns should increase 10 times than that of the 2NSDO. Therefore, the 2NSDO achieves a larger damping ratio with a much smaller demand for the perimeter column stiffness compared with the 2CDO and the CDO.

As shown in Fig. 7(d)-Fig. 7(f), the use of the 2NSDO decreases the first modal frequency if the outrigger damping is small. It is because that the NSD reduces the static stiffness of the structure. With very large outrigger damping, the frequencies of the 2NSDO are close to that

Table 1. Default parameter for different outrigger systems

	c_1	c_2	α	β	η_1	η_2	k_{NS2} / k_{NS1}
2NSDO	0~0.1	0~0.1	0.55	5.0	–0.35	–0.23	0.8
2CDO	0~0.1	0~0.1	0.55	5.0	0	0	-
1NSDO	0~0.1	0	0.55	5.0	–0.35	-	-
1CDO	0~0.1	0	0.55	5.0	0	-	-



(a) The 1st modal damping ratio (b) The 2nd modal damping ratio

(c) The 3rd modal damping ratio (d) The 1st modal frequency

(e) The 2nd modal frequency (f) The 3rd modal frequency

Figure 7. Modal damping ratios and frequencies for the 2NSDO,2CDO,1NSDO, and 1CDO structures with the variance of normalized outrigger damping.

of the 2CDO. The reason is that the stroke of the viscous damper and the negative stiffness spring is going to be locked at very large outrigger damping. In this case, the behavior of the 2NSDO is also similar to a 2CDO. When $c = 0$, the normalized frequency of 2NSDO is smaller than that of 1NSDO, which means 2NSDO further reduces the static stiffness of the structures compared with 1NSDO.

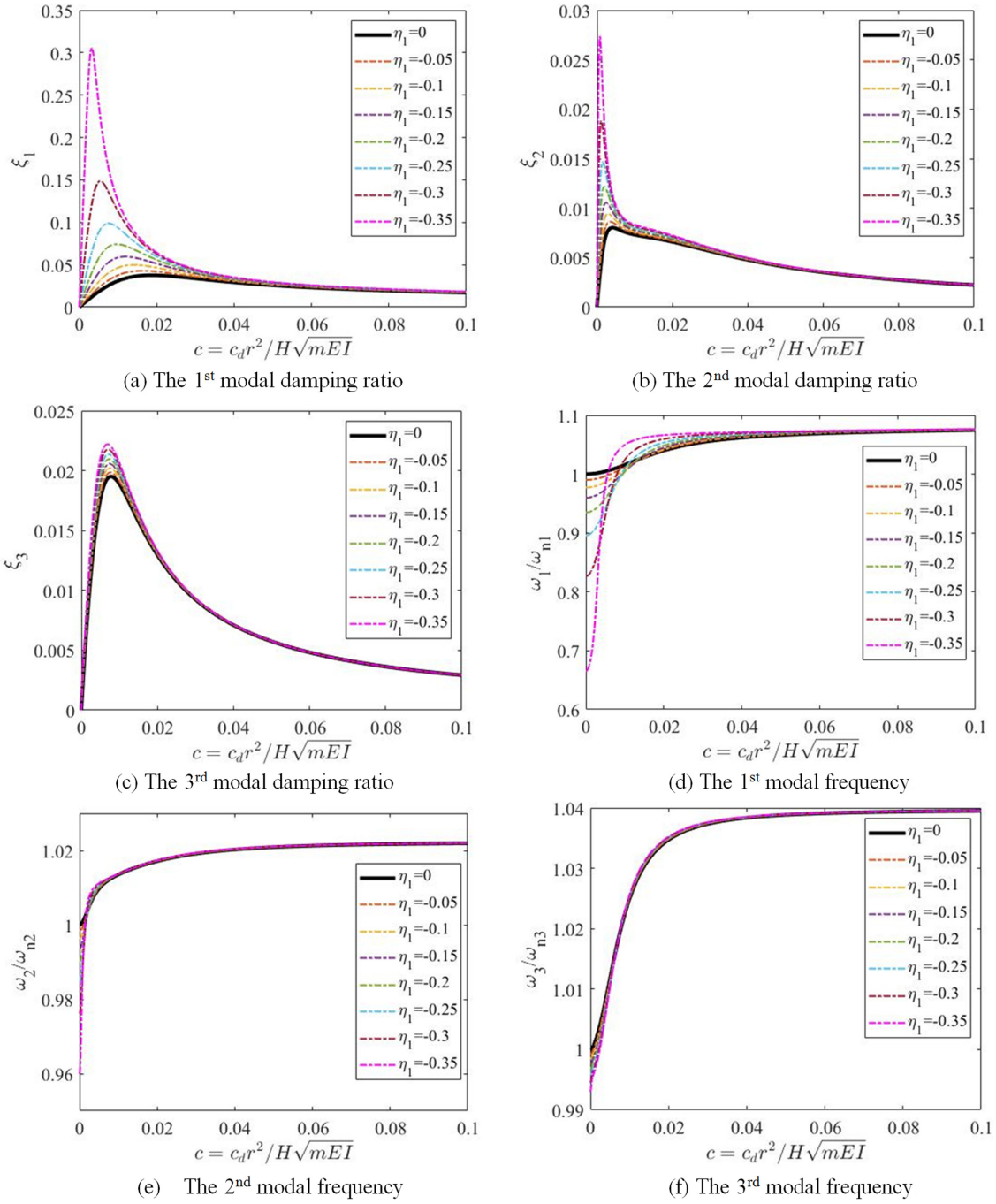
The influence of the 2NSDO on higher modes' frequencies has a similar trend as that on the first mode but varies within a very small range (within 2%). Moreover, the damping ratios for higher modes are much smaller than that for the first mode. This is because the default outrigger's position is at the middle of the structure and can not effectively control the vibration of higher modes.

3.3.2 Influence of Negative Stiffness

Fig. 8 shows the damping ratio and frequency of the first three mode under stiffness scale $k_{NS2} / k_{NS1} = 0.8$ with

the variation of normalized outrigger damping c and the first negative stiffness ratio $|\eta_1|$. It is obvious that the increase of $|\eta_1|$ leads to a considerable promotion in the maximum achievable damping ratio. As for the static frequency, the increase of $|\eta_1|$ further reduces the static structural frequency (i.e., a curve's value at $c = 0$ in Fig. 8(d)) but leads to the same value at large outrigger damping.

Fig. 9 presents the maximum achievable modal damping ratio of the first mode (i.e., the peak values of the curves in Fig. 7(a)) of 2NSDO and the static frequency ratio (i.e., a curve's value at $c = 0$ in Fig. 7(d)) of 2NSDO with the variation of the stiffness scale k_{NS2}/k_{NS1} and the first negative stiffness ratio $|\eta_1|$. The $|\eta_1|$ in each stiffness scale k_{NS2}/k_{NS1} has its own reasonable scope: if the $|\eta_1|$ is larger than this scope, the calculation of Eq.(1 will not converge (Duan 2021). It is evident that the increase of $|\eta_1|$ leads to a considerable improvement in the maximum achievable damping ratio. And with the same $|\eta_1|$,



(a) The 1st modal damping ratio

(b) The 2nd modal damping ratio

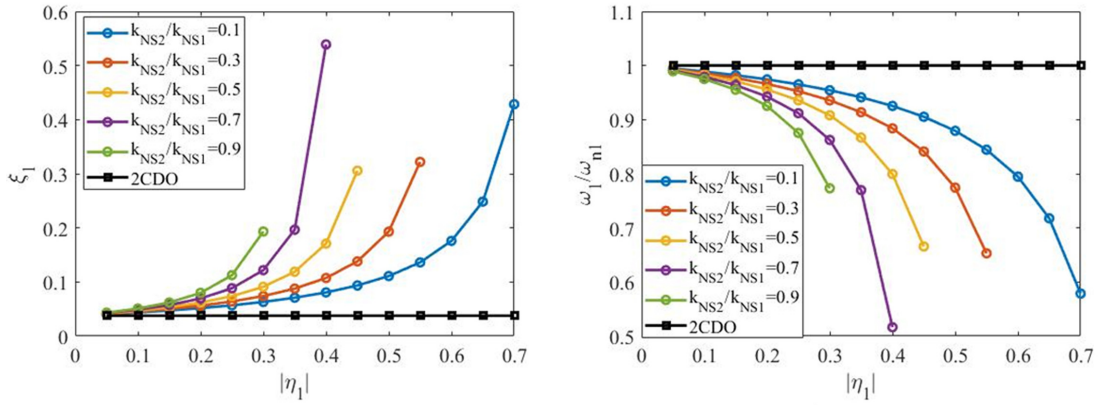
(c) The 3rd modal damping ratio

(d) The 1st modal frequency

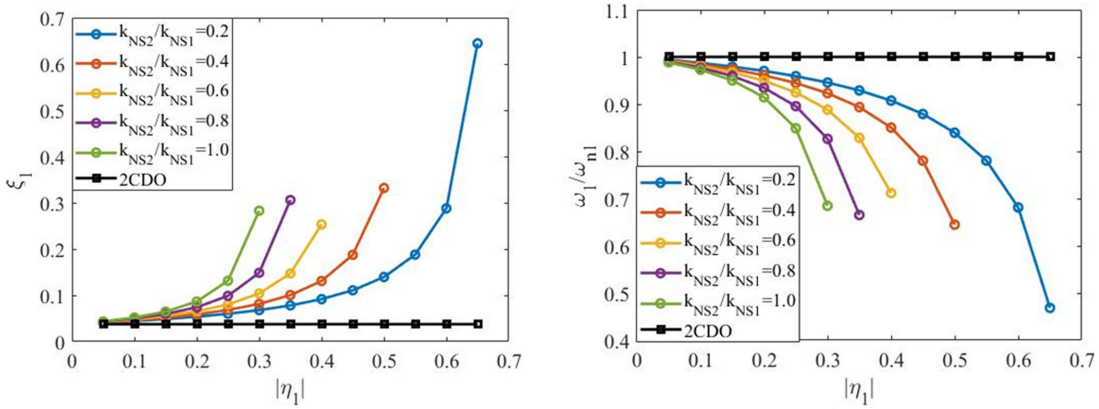
(e) The 2nd modal frequency

(f) The 3rd modal frequency

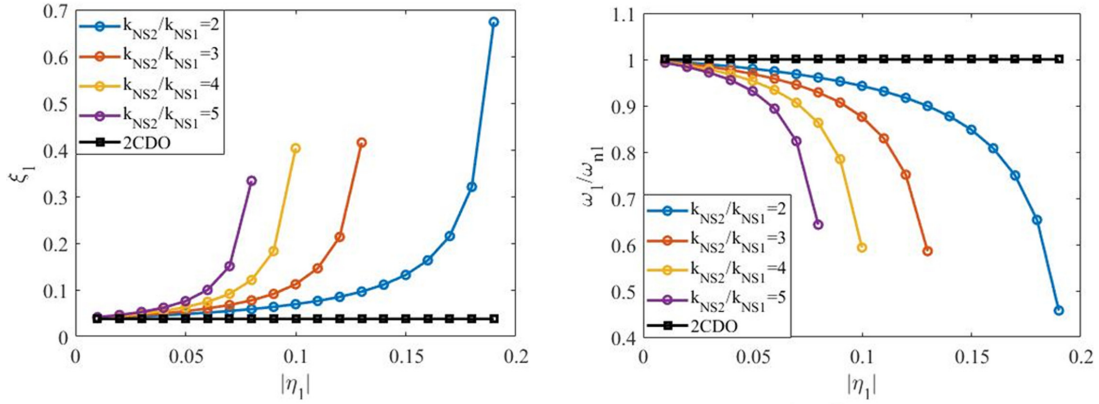
Figure 8. Modal damping ratios and frequencies for the 2NSDO with the variance of normalized outrigger damping and negative stiffness ratio.



(a) The modal damping ratios and the static-frequencies ratios (k_{NS2}/k_{NS1}=0.1~0.9)



(b) The modal damping ratios and the static-frequencies ratios (k_{NS2}/k_{NS1}=0.2~1)



(c) The modal damping ratios and the static-frequencies ratios (k_{NS2}/k_{NS1}=2~5)

Figure 9. Influence of the stiffness scale k_{NS2} / k_{NS} and the first negative stiffness ratio on the maximum achievable modal damping ratios of first mode and the static frequencies ratios.

the maximum achievable damping ratio of first mode increases as the stiffness scale k_{NS2} / k_{NS1} increases. In contrast, the static frequency ratio of the structure decreases as the $|\eta_1|$ increases, which results from the weakening of the static stiffness caused by the negative stiffness. And, the static frequency ratio of the structure decreases as the stiffness scale k_{NS2} / k_{NS1} increases with identical $|\eta_1|$.

3.3.3. Influence of Stiffness Ratio of a Core Tube–to-Column

Fig. 10 shows the damping ratio and frequency of the first mode under k_{NS2} / k_{NS1} = 0.8 with the variation of normalized outrigger damping c and the stiffness ratio of core tube-to-column β. The maximum achievable damping ratio for 2NSDO increases as the β decreases. On the contrary, the static structural stiffness decreases as the β decreases. These rules are the same as that of the 1NSDO structures (Wang and Nagarajaiah et. al. 2021).

As shown in Fig. 11 the maximum achievable modal damping ratio of the first mode (i.e., the peak values of the curves in Fig. 10(a) increases as the negative stiffness ratio $|\eta_1|$ increases under the same β. In contrast, the

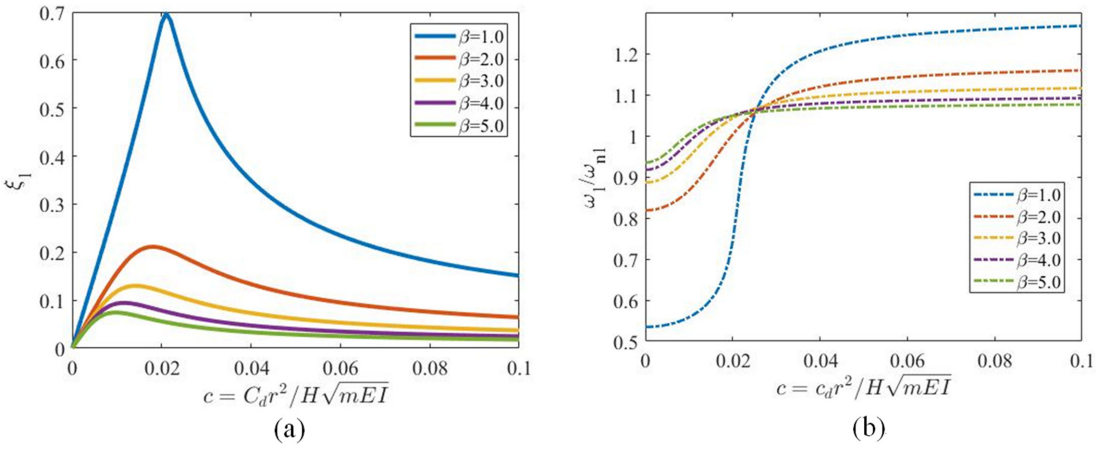


Figure 10. The first modal damping ratios and frequencies for the 2NSDO with the variance of normalized outrigger damping and stiffness ratio of a core tube-to-column: (a) 1st modal damping ratio, (b) 1st modal frequency.

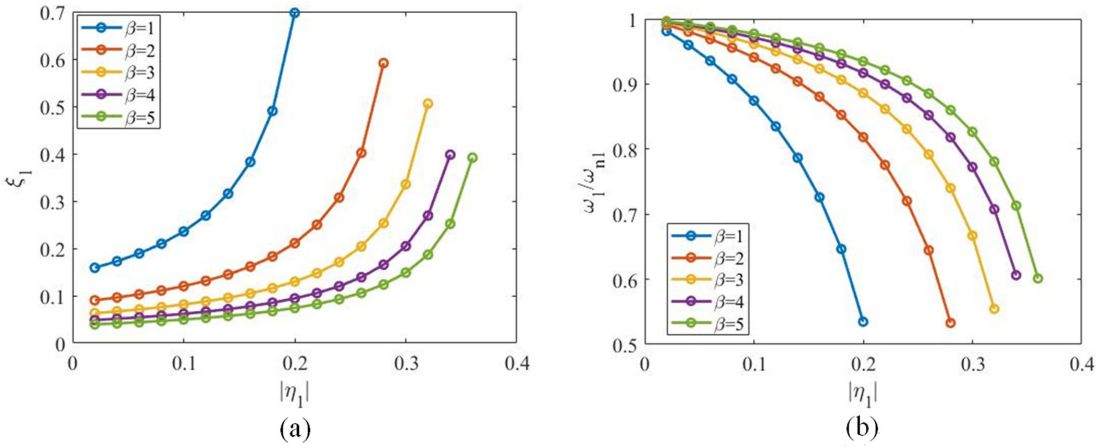
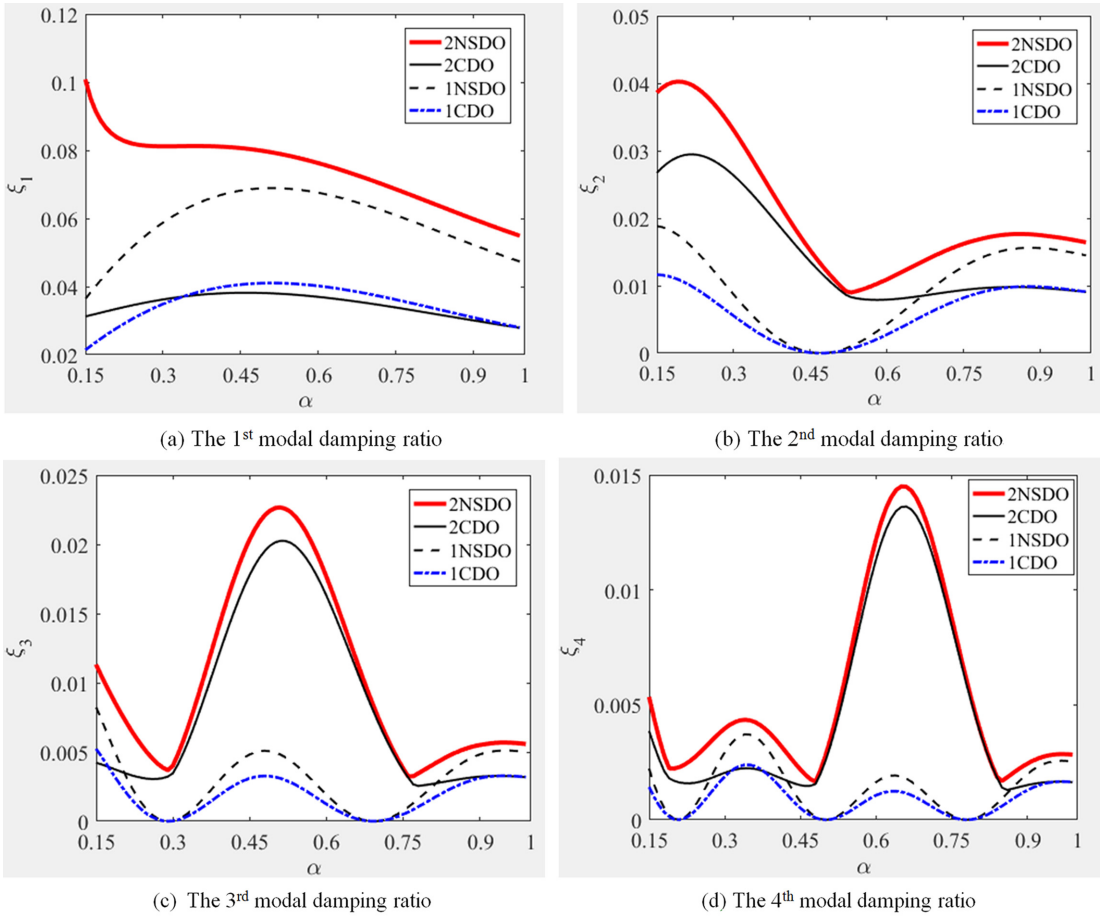


Figure 11. The maximum achievable first modal damping ratios and static frequencies for the 2NSDO with the variance of stiffness ratio of a core tube-to-column and the first negative stiffness ratio: (a) 1st maximum achievable modal damping ratio, (b) static-frequencies ratios.

static frequencies (i.e., a curve's value at $c = 0$ in Fig. 10(b)) decreases as the $|\eta_1|$ decreases with the same β. These phenomena are the same as that of the 1NSDO structures (Wang et al. 2021).

3.3.4 Influence of Outrigger Position

In this part, the stiffness scale k_{NS2} / k_{NS1} of 2NSDO is chosen as 0.2. In this paper, the lower NSDO is called the first NSDO, and the upper NSDO is called the second NSDO. The second outrigger is fixed at the top of the core tube in this parametric study, so only the normalized position ratio for the first outrigger α is the position variable. Fig. 12 presents the maximum achievable modal damping ratio distribution of height. Because the first outrigger usually should be installed too close to the ground, the scope of the α is 0.15~1. All the curves have a waveform in Fig. 12. For each modal, with reference to the wave curve of 1NSDO, the wave crest appears at the region of the second NSDO. If the first NSDO is located at the same crest of the second NSDO, the modal damping ratio has minor increases. While if the first NSDO is located at the wave crest next to the wave crest with the second NDSO, the maximum damping ratio can be achieved. The 2NSDO obtains the absolute maximum achievable damping ratio with a value of 10% for the first mode when the outrigger is placed at $\alpha = 0.15$, which is larger than the absolute maximum achievable damping ratio for the first mode of 1NSDO (5%). In addition, the absolute maximum achievable damping ratio for each mode of 2NSDO structure is larger than that of the structure with one NSDO. Therefore, an extra NSDO can improve the damping ability of the structure with one NSDO. For each mode, the 2NSDO has the similar outrigger position to achieve the absolute maximum achievable damping ratio as the 2CDO does, despite the damping ratio provided by the 2CDO being much lower that provided by the 2NSDO. The modal damping ratios of 2NSDO for all modes are the largest compared with



(a) The 1st modal damping ratio (b) The 2nd modal damping ratio

(c) The 3rd modal damping ratio (d) The 4th modal damping ratio

Figure 12. The maximum achievable modal damping ratios distribution over the height.

that of the 1CDO, 2CDO, and 1NSDO.

Fig. 13 shows the distribution of the static-frequencies ratio over the height of each mode, and the dotted line represents the position of the wave crests and valleys of the modal damping ratio curve. In terms of the static-frequencies ratio, the 2NSDO's static-frequencies ratios are lower than that of the 1CDO, 2CDO, and 1NSDO, as shown in Fig 13. The curves of the 2NSDO have a waveform. The positions corresponding to the wave crests of the static-frequencies ratios are similar to the positions corresponding to the valleys of the maximum damping ratios. On the contrary, the positions corresponding to the valleys of the static frequency are similar to the position corresponding to the wave crests of the maximum damping ratios.

4. Vibration Mitigation Effect of 2NSDO Under Fluctuating Wind

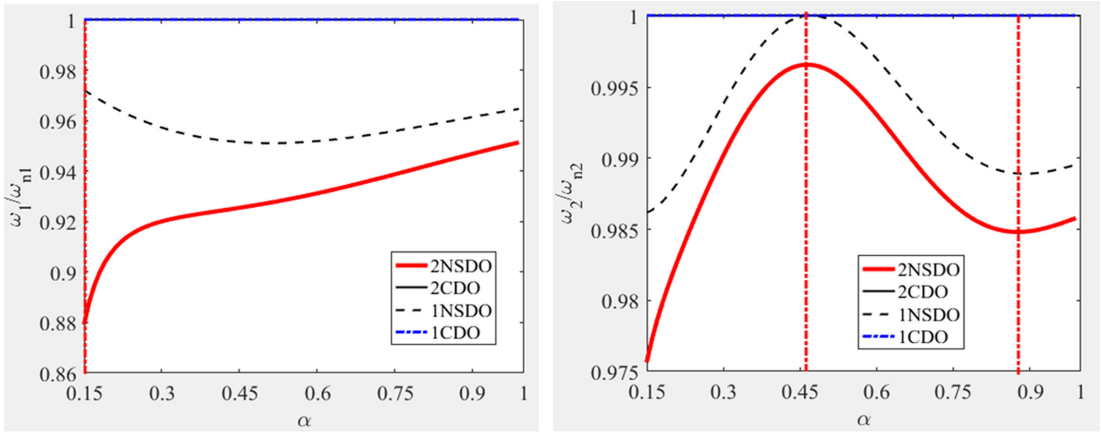
4.1. Description of Structural model

A 40-story structure with the height of 160 m is adopted as a numerical example for the 2NSDO structure to investigate its performance under fluctuating wind. As shown in Fig. 14, 8 perimeter columns are located around the core tube, and the distance between the column and core tube is 0.15 m. The main structure parameters are as follows: a bending stiffness of core tube $EI = 1.667 \times 10^{13}$ Nm^2, distributed mass $m = 11.56 \times 10^4$ kg/m, structural height $H = 160$ m, and outrigger length $r = 8$ m. The detailed information can be search in the reference of Duan.

The detailed parameters of 2NSDO, 2CDO,1NSDO, and 1CDO are shown in Table 2. The viscous coefficient of each structure is the value that corresponding to the maximum achievable modal damping ratio of the first mode for each structure. The η_1 and η_2 are selected from the value that can achieve the maximum achievable modal damping ratio of the first mode. And the α_1 and α_2 are selected according to the existing engineering (Duan 2021). For the tall buildings with double outriggers, the normalized position ratio for the first outrigger is usually in the range of 0.3~0.5. And the normalized position ratio for the second outrigger is usually in the range of 0.6~0.8.

4.2. Fluctuating wind response

The responses of the structural model subjected to the fluctuating wind are obtained by the finite-element method of Wang et al.'s work (Wang et al. 2021). In this analysis, the Davenport spectrum is selected as the target wind



(e) The 1st modal frequency (f) The 2nd modal frequency

(g) The 3rd modal frequency (h) The 4th modal frequency

Figure 13. The static-frequencies ratios distribution over the height.

Table 2. Detailed parameters of 2NSDO, 2CDO,1NSDO, and 1CDO

	c_1	c_2	α	β	η_1	η_2	k_{NS2} / k_{NS1}	c_1
2NSDO	0.0258	0.0258	0.35	0.7	2.17	–0.2	–0.16	0.2
2CDO	0.0538	0.0538	0.35	0.7	2.17	0	-	-
1NSDO	0.1052	0	0.35	-	2.17	–0.2	-	-
1CDO	0.1052	0	0.35	-	2.17	0	-	-

spectrum for the wind load. The wind record is produced using the autoregressive method, and the simulated wind load is applied on each degree-of-freedom. The value of the wind-excited responses of the 2NSDO 2CDO, 1NSDO, and 1CDO under one typical wind record are summarized in Fig. 3 and Table 3.

As shown in Fig. 15, the peak acceleration responses of

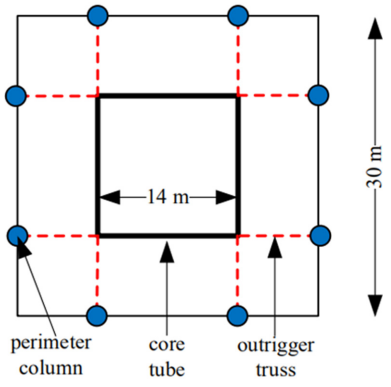


Figure 14. Configuration of the structural model.

Table 3. Response of 2NSDO, 2CDO,1NSDO, and 1CDO

Structure systems	Peak response	
	Top acceleration (m/s^2)	Top drift ratio (10^{-3})
2NSDO	0.1657	0.494
2CDO	0.1998 (–17.1%)	0.469 (5.3%)
1NSDO	0.2804 (–40.9%)	0.486 (1.4%)
1CDO	0.3178 (–47.9%)	0.510 (3.2%)

Note: Values in the parenthesis represent the response relative differences of 2NSDO compared to different outrigger structures.

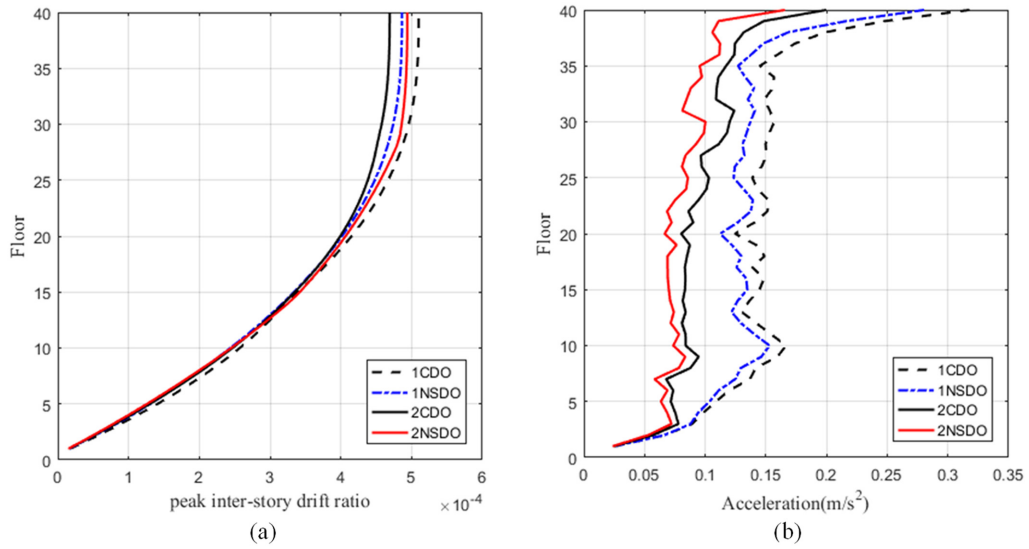


Figure 15. Response of the 40-story building under fluctuating wind load: (a) peak interstory drift (m); (b) peak acceleration.

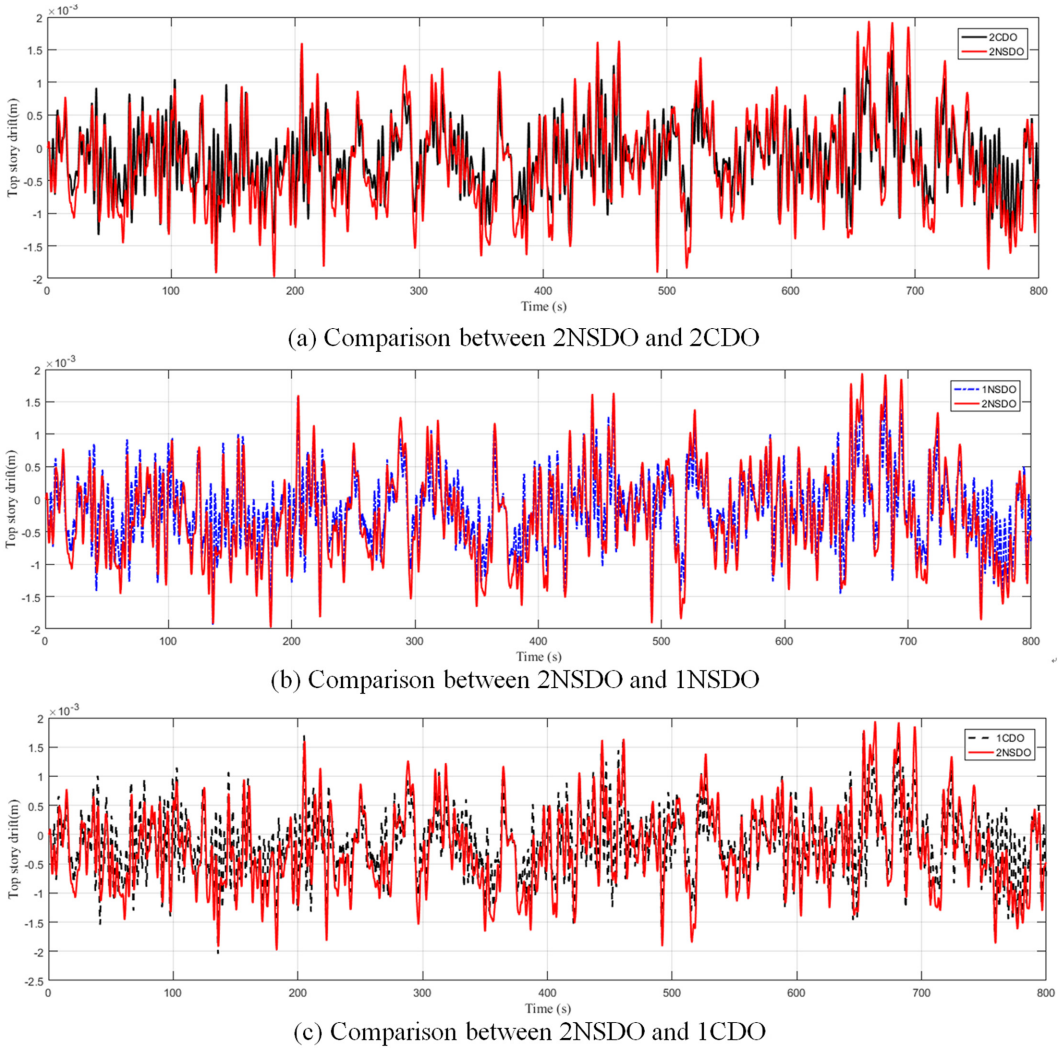
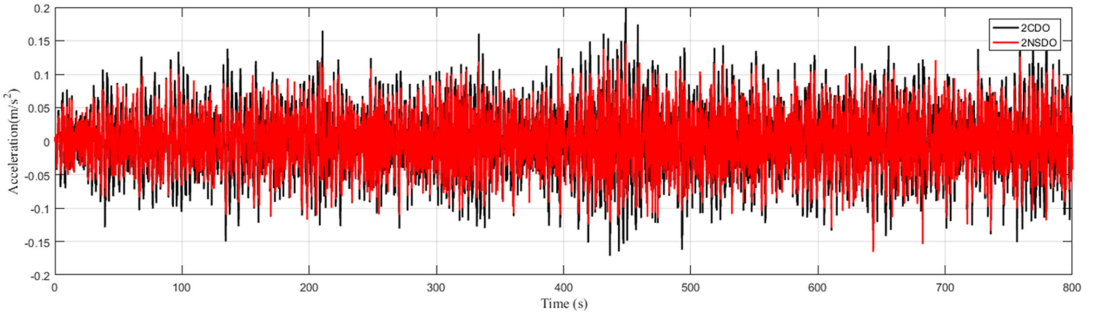


Figure 16. Time history of the 40th-story's drift under fluctuating wind.

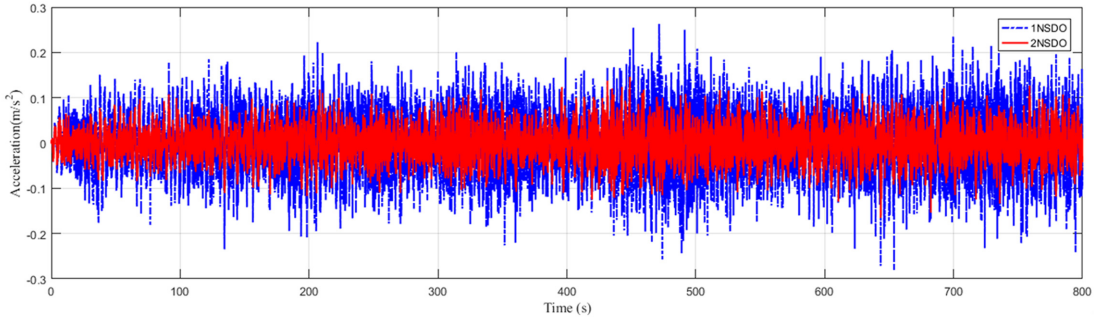
2NSDO significantly smaller than that of the 1NSDO, 2CDO, and 1CDO, due to its large modal damping ratio. For example, the peak acceleration response of the 2NSDO is smaller than that of the 1CDO by over 45%. And the peak acceleration response of the 2NSDO is smaller than that of the 1NSDO by over 40% using 24.5% of the expenses of the outrigger damping coefficient of the 1NSDO. And the peak acceleration response of the 2CDO can be further reduced by over 15 % at the fewer expenses of the outrigger damping coefficient. As for the interstory drift ratio responses, because the negative stiffness weakens the static stiffness of the structure, the 2NSDO degrades the displacement mitigation performance of the 2CDO, and the top drift ratio is amplified by 5.3%. Compared with 1NSDO, the 2NSDO amplifies the top drift ratio by 1.4%. The amplification ratio of interstory drift ratio caused by the 2NSDO is acceptable in engineering.

Generally, the structural comfort level for customers and the performance of some highly sensitive equipment/ devices are highly dependent on the acceleration response level. Hence, from the standpoint of practical application, the 2NSDO is useful in improving the structural comfort and the performance of acceleration-sensitive equipment. The 2NSDO uses 52% of the expenses of the outrigger damping coefficient of the 2CDO to achieve a better acceleration mitigation performance. Therefore, even though the 2NSDO amplifies the interstory drift ratio slightly, the 2NSDO still has an application value in engineering.

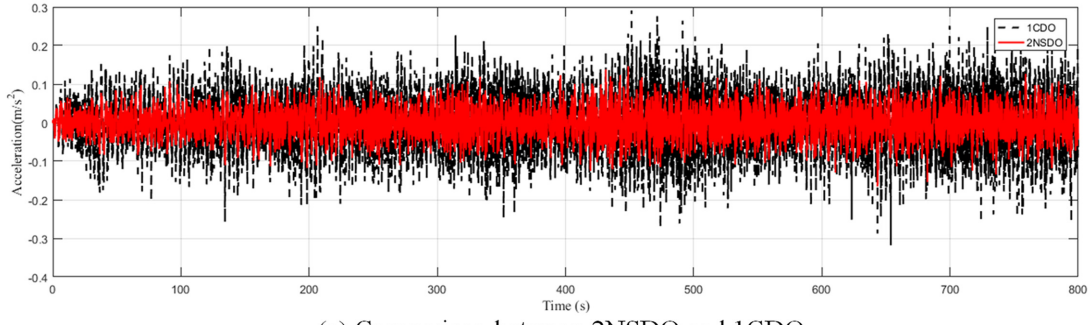
Fig. 16 and Fig. 17 show the time history results of the 40th-story's drift and acceleration under fluctuating wind record. The 2NSDO reduces the acceleration response for the whole duration compared with the 2CDO. Besides, it is obvious that the 2NSDO substantially reduces the acceleration responses for the whole duration compared with 1NSDO and 1CDO. The vibration period of 2NSDO, 2CDO, 1NSDO, and 1CDO are the same in terms of time history results of the 40th-story's drift.



(a) Comparison between 2NSDO and 2CDO



(b) Comparison between 2NSDO and 1NSDO



(c) Comparison between 2NSDO and 1CDO

Figure 17. Time history of the 40th-story's acceleration under fluctuating wind.

5. Conclusions

In this paper, the dynamic characteristics of tall building structures with double negative stiffness damped outriggers (2NSDO) are parametrically studied. Then the vibration mitigation effect of 2NSDO is evaluated under the fluctuating wind load by time-history analysis. The major findings are summarized as follows:

1) Compared with the 1NSDO, the 2NSDO structure only needs 46.6% of the negative stiffness of the 1NSDO to achieve the same first modal damping ratio of 30%, which largely simplifies the application of NSDO.
2) Compared with the 2CDO, the 2NSDO significantly improves the modal damping ratio for each structural mode with much less consumption of the outrigger damping coefficient
3) The maximum achievable modal damping ratio of the first mode of 2NSDO significantly increases with the increase of the negative stiffness ratio between the first NSDO and the second NSDO.
4) The maximum achievable modal damping ratio of the first mode of 2NSDO structures increases as the stiffness ratio of core tube-to-column decreases.
5) For the 2NSDO structure with one NSDO fixed on the top of the core tube, the 2NSDO has the same optimal outrigger position, as the 2CDO does, to achieve the absolute maximum achievable damping ratio for each mode. Therefore, adding a proper negative stiffness device and outrigger damping is applicable to retrofit the 2CDO without changing the position of outriggers.
6) Under fluctuating wind load, compared with the 2CDO and 1NSDO, the 2NSDO can further mitigate the acceleration responses at fewer expenses of the outrigger damping coefficient with an acceptable amplification of inter-story drift.

Acknowledgments

Financial support from the State Key Laboratory of Disaster Reduction in Civil Engineering of China (Grant No. SLDRCE19-B-16) is greatly acknowledged by authors.

References

Antoniadis, I. A., S. A. Kanarachos, K. Gryllias, and I. E. Sapountzakis. 2016. “KDamping: A stiffness based vibration absorption concept.” J. Vib. Control 24(3), 588-606.

Chen, L., L. Sun, and S. Nagarajaiah. 2015. “Cable with discrete negative stiffness device and viscous damper: Passive realization and general characteristics.” Smart Struct. Syst. 15(3), 627-643.

Duan N. L. (2021) Study on Wind-induced Structural Vibration of Tall Buildings with Negative Stiffness Damped Outriggers. Tongji University.

Iemura, H., and M. H. Pradono. 2009. “Advances in the development of pseudo-negative-stiffness dampers for seismic response control.” Struct. Control Health Monit. 16(8), 784-799.

Kwon, I. Y., H. T. Yang, P. K. Hansma, and C. J. Randall. 2016. “Implementable bio-inspired passive negative spring actuator for full-scale structural control under seismic excitation.” J. Struct. Eng. 142(1), 04015079.

Nagarajaiah, S. 2009. “Adaptive passive, semiactive, smart tuned mass dampers: Identification and control using empirical mode decomposition, Hilbert transform, and short-term Fourier transform.” Struct. Control Health Monit. 16(7-8), 800-841.

Pasala, D. T. R., A. A. Sarlis, A. M. Reinhorn, S. Nagarajaiah, M. C. Constantinou, and D. Taylor. 2015. “Apparent weakening in SDOF yielding structures using a negative stiffness device: Experimental and analytical study.” J. Struct. Eng. 141(4), 04014130.

Pasala, D. T. R., A. A. Sarlis, S. Nagarajaiah, A. M. Reinhorn, M. C. Constantinou, and D. Taylor. 2013. “Adaptive negative stiffness: New structural modification approach for seismic protection.” J. Struct. Eng. 139(7), 1112-1123.

Pasala, D. T. R., S. Nagarajaiah, D. Taylor, A. M. Reinhorn, M. C. Constantinou, and A. A. Sarlis. 2014. “Simulated bilinear-elastic behavior in a SDOF elastic structure using negative stiffness device: Experimental and analytical study.” J. Struct. Eng. 140(2), 04013049

Qu, C., H. N. Li, L. Huo, and T. H. Yi. 2017. “Optimum value of negative stiffness and additional damping in civil structures.” J. Struct. Eng. 143(8), 04017068.

Sarlis, A. A., D. T. R. Pasala, M. C. Constantinou, A. M. Reinhorn, S. Nagarajaiah, and D. P.Taylor. 2013. “Negative stiffness device for seismic protection of structures.” J. Struct. Eng. 139(7), 1124-1133.

Sapountzakis, E. J., P. G. Syrimi, I. A. Pantazis, and I. A. Antoniadis. 2017. KDamper concept in seismic isolation of bridges with flexible piers.” Eng. Struct. 153(Dec), 525-539.

Shi, X., and S. Zhu. 2015. “Magnetic negative stiffness dampers.” Smart Mater. Struct. 24(7), 072002.

Sun, F. F., Wang, M., Nagarajaiah, S. (2021). Multi-objective optimal design and seismic performance of negative stiffness damped outrigger structures considering damping cost. Engineering Structures, 229, 111615.

Sun, T., Z. Lai, S. Nagarajaiah, and H. Li. 2017. “Negative stiffness device for seismic protection of smart base isolated benchmark building.” Struct. Control Health Monit. 24(11), e1968.

Tan, P., C. J. Fang, C. M. Chang, B. F. Spencer, and F. L. Zhou. 2015. “Dynamic characteristics of novel energy dissipation systems with damped outriggers.” Eng. Struct. 98(Sep), 128-140.

Wang, M., Sun, F. F., and Jin H. J. 2018. “Performance evaluation of existing isolated buildings with supplemental passive pseudo-negative stiffness devices.” Eng. Struct.

Wang, M., Sun, F., and Nagarajaiah, S. (2019). Simplified optimal design of mdof structures with negative stiffness amplifying dampers based on effective damping. The Structural Design of Tall and Special Buildings.

Wang, M., Sun, F. F., Yang, J. Q., and Nagarajaiah, S. (2019). Seismic protection of sdof systems with a negative stiffness amplifying damper. Engineering Structures, 190(JUL.1), 128-141.

Wang, M., Nagarajaiah, S., and Sun, F. F. (2020). Dynamic characteristics and responses of damped outrigger tall buildings using negative stiffness. Journal of Structural Engineering, 146(12), 04020273.